

Unscheduled epigenetic modifications cause genome instability and sterility through aberrant R-loops following starvation

Bing Sun¹*, McLean Sherrin and Richard Roy¹*

Department of Biology, McGill University, Montreal, Quebec H3A 1B1, Canada

Received October 25, 2022; Editorial Decision November 12, 2022; Accepted December 09, 2022

ABSTRACT

During starvation, organisms modify both gene expression and metabolism to adjust to the energy stress. We previously reported that *Caenorhabditis elegans* lacking AMP-activated protein kinase (AMPK) exhibit transgenerational reproductive defects associated with abnormally elevated trimethylated histone H3 at lysine 4 (H3K4me3) levels in the germ line following recovery from acute starvation. Here, we show that these H3K4me3 marks are significantly increased at promoters, driving aberrant transcription elongation resulting in the accumulation of R-loops in starved AMPK mutants. DNA-RNA immunoprecipitation followed by high-throughput sequencing (DRIP-seq) analysis demonstrated that a significant proportion of the genome was affected by R-loop formation. This was most pronounced in the promoter–transcription start site regions of genes, in which the chromatin was modified by H3K4me3. Like H3K4me3, the R-loops were also found to be heritable, likely contributing to the transgenerational reproductive defects typical of these mutants following starvation. Strikingly, AMPK mutant germ lines show considerably more RAD-51 (the RecA recombinase) foci at sites of R-loop formation, potentially sequestering them from their roles at meiotic breaks or at sites of induced DNA damage. Our study reveals a previously unforeseen role of AMPK in maintaining genome stability following starvation. The downstream effects of R-loops on DNA damage sensitivity and germline stem cell integrity may account for inappropriate epigenetic modification that occurs in numerous human disorders, including various cancers.

INTRODUCTION

In most organisms, a highly conserved enzyme called adenosine monophosphate (AMP)-activated protein kinase (AMPK) acts as an important metabolic master regulator through its ability to sense reduced energy levels (1). In situations of stress such as starvation, AMPK ensures that energy is appropriately allocated to all essential cellular processes (1–3). As embryogenesis terminates, the emergent *Caenorhabditis elegans* L1 larvae will only begin to develop post-embryonically if nutritional resources are adequate. If food is limiting, the animal enters a quiescent, nondeveloping stage called the L1 diapause and can remain in this state for up to 2 weeks. In the diapause, all cell divisions are arrested, transcription and translation are maintained at a minimum, and the animals wait for an improvement in growing conditions to trigger the changes typical of the onset of postembryonic development.

We noted previously that following recovery from acute starvation as emergent L1 larvae, *C. elegans* that lack AMPK are often sickly, have reduced brood sizes or are sterile (2). Intriguingly, these reproductive defects are transmitted to subsequent generations of animals that were never starved, suggesting that a molecular memory of the stress is transmitted to future generations when this enzyme is disrupted. Later generations show spontaneous somatic mutant phenotypes, much like mutant animals that lack histone demethylase activity (4,5), and often become sterile after one to several (up to 10) generations. These transgenerational reproductive defects can also occur at very low frequency in wild-type (WT) animals that are starved for extended durations (6). This suggests that the epigenetically inherited reproductive defects documented in the descendants of mutants lacking AMPK very likely reflect the extreme effects of starvation on the germ line, although they occur after a much shorter delay in AMPK mutants.

Transgenerational epigenetic inheritance has been observed in several contexts in *C. elegans*, and the progressive “mortalization” of the germ line is often associated with aberrant changes in the histone modifications typically

*To whom correspondence should be addressed. Email: bingsun245@gmail.com

Correspondence may also be addressed to Richard Roy. Tel: +1 514 398 6437; Email: richard.roy@mcgill.ca

Present address: Bing Sun, RNA Therapeutics Institute, University of Massachusetts Medical School, 368 Plantation Street, Worcester, MA 01605, USA.

present in the affected germ cells (7–9). In animals lacking AMPK signaling, starvation results in a significant accumulation of trimethylated histone H3 at lysine 4 (H3K4me3) in the primordial germ cells (PGCs) of post-L1 diapause, while the levels of other chromatin marks are not appreciably different. In contrast, the levels of H3K4me3 present in the PGCs of WT animals are quite low during starvation, consistent with their low transcriptional activity. This change in the H3K4me3 levels in the PGCs is due to the misregulation of the Mixed Lineage Leukemia (MLL)/SET-2/Complex Proteins Associated with Set1 (COMPASS)-like complex. This inappropriate activation of the COMPASS-like complex results in the unscheduled activation of transcriptional elongation during a period when gene expression as a whole should be attenuated (2,10).

Our previous study revealed that misregulated transcriptional elongation contributes to the sterility of post-L1 diapause AMPK mutants (2). Efficient transcriptional elongation only occurs following multiple changes within the post-initiation RNA polymerase II (Pol II) complex that enhances RNA processing. In the absence of these components, the elongating complex pauses until these contingencies are satisfied (11–13). In some cases, the nascent RNA associated with these stalled complexes can thread back into the transcription bubble, where it can base pair with the noncoding strand of DNA. These three-stranded structures harboring an RNA:DNA hybrid are referred to as R-loops, and they are abundant non-B DNA structures that often form during transcriptional pausing (14). The persistence of R-loops is associated with replication/transcription conflicts that can result in DNA damage. Furthermore, they are also a source of genome instability resulting from single nucleotide changes catalyzed by DNA modifying enzymes, such as cytosine deaminases, that can access the vulnerable single-stranded DNA (15,16).

Here, we describe that the aberrant H3K4me3-induced transcription elongation that occurs in starved AMPK mutants results in the accumulation of R-loops at numerous loci and is most pronounced at the promoter–transcription start site (TSS) regions of the affected genes. The observed increase in R-loop frequency is transmissible into subsequent generations and likely contributes to the transgenerational reproductive defects typical of AMPK mutants following starvation. RAD-51 foci accumulate at sites of R-loop formation in post-L1 diapause AMPK mutant germ lines, while introducing extra copies of RAD-51 could partially restore fertility in these animals. Taken together, our data suggest that AMPK blocks the inappropriate deposition of H3K4me3 marks during this period of energy stress and in its absence these ‘ectopic’ chromatin marks result in untimely transcriptional elongation and consequent R-loop formation. These structures eventually sequester RAD-51, limiting the availability of this important DNA repair factor and thus compromising its roles in both the DNA damage response and meiosis.

MATERIALS AND METHODS

Caenorhabditis elegans strains and genetics

Caenorhabditis elegans were cultured at 20°C on OP50. Strains used in this study include the following: Bristol

N2, *aak-1(tm1944)* III; *aak-2(ok524)* X, *thoc-2(tm1310)* III/*hT2[bli-4(e937) let-2(q782) qIs48]* (I;III) and *smIs34*.

Reagents and antibodies

Methyl methanesulfonate (MMS, 129925, Sigma-Aldrich), hydroxyurea (HU, H8627, Sigma-Aldrich), Agencourt AMPure XP (A63880, Beckman Coulter), 4,6-diamidino-2-phenylindole (DAPI, 10236276001, Roche), Halt Protease and Phosphatase Inhibitor Cocktail (1861281, Thermo Scientific), VECTASHIELD Antifade Mounting Medium (H-1000, Vector Laboratories), RNase H (M0297, NEB) and cycloheximide (CHX, 1041–1, BioVision). The following antibodies were used: anti-DNA–RNA hybrid, clone S9.6 (MABE1095, Millipore), anti-RAD-51 (gift from Monique Zetka), anti-H3K4me3 (ab8580, Abcam), anti-Pol II S2 (RNA Pol II phosphorylated serine 2; ab5095, Abcam), Goat anti-Rabbit IgG (H + L) highly cross-adsorbed secondary antibody, Alexa Fluor 488 (A-11034, Invitrogen) and Goat anti-Mouse IgG (H + L) highly cross-adsorbed secondary antibody, Alexa Fluor 594 (A-11032, Invitrogen).

ChIP-Seq and DRIP-seq

L1 hatchlings were maintained for 3 days in a sterile M9 buffer without bacteria (2). After this period, L1 larvae were transferred to nematode growth media (NGM) plates and fed for two generations until F₂ adults were harvested to generate extracts for both chromatin immunoprecipitation (ChIP) and DRIP. Immunoprecipitation was performed from three biological repeats. DRIP in *C. elegans* was performed as described with minor modifications (17). Primers used for DRIP-qPCR are as follows: *tig-3* (forward: 5'-ACTCCAAATGCTCTAAGT ACAACTG-3', reverse: 5'-ACACAGTGTGCTCCACAG-3'); *K07C5.6* (forward: 5'-CCTTCTCGCGTTCTTTTT CTTTTTC-3', reverse: 5'-CAAAGTTCGGAAGTTAGT AGAGAAGAC-3'); *cit-1.2* (forward: 5'-GCTCTTTATT TGCGTTCAATTCCTG-3', reverse: 5'-GTTCGACAACA AGAGTGGAAACC-3') and *rrn-3.56* (forward: 5'-CCCA CAGATCTACTATATTAATGTGCC-3', reverse: 5'-TCCCCGCTTGACACTGT-3').

The libraries were prepared and sequenced by the Institute for Research in Immunology and Cancer (IRIC) in Montreal, Canada. The sequencing data were obtained using an Illumina Nextseq instrument, and data were analyzed with the ChIP-seq pipeline implemented by the Canadian Centre for Computational Genomics. Reads were trimmed from the 3' end to have a Phred score of at least 30. Illumina sequencing adapters were removed from the reads, and all reads were required to have a length of at least 50 bp. Trimming and clipping were performed using Trimmomatic (18). The filtered reads were aligned to the *cell1* genome (*Caenorhabditis elegans* assembly WBcel235). Each readset was aligned using Burrows–Wheeler Aligner algorithm (19), which creates a Binary Alignment Map file (.bam). Then, all readset BAM files from the same sample were merged into a single global BAM file using Picard. Base quality filtering of the aligned reads was then performed based on the quality of the BAM file, where each

alignment file per sample was filtered using SAMtools (20). All alignments with MAPPING Quality (MAPQ) <20 and samflag 4 (read unmapped) are excluded from the resulting file in BAM format. Duplicated aligned reads that have the same 5' alignment positions were made with Picard. All but the best pair (based on alignment score) was marked as a duplicate in the BAM file. Duplicate reads were excluded from subsequent analysis.

To facilitate the analysis of ChIP-Seq, the HOMER software (21) was used to transform the sequence alignment into a platform-independent data structure representing the experiments. All relevant information about the experiment was organized into a 'Tag Directory'. During the creation of tag directories, several quality control routines were run to help provide information and feedback about the quality of the experiment. BedGraph track format files were generated from the aligned reads using HOMER. Peaks were called using MACS software (22) and were annotated with HOMER using RefSeq annotations. Gene ontology and genome ontology analyses are also performed at this stage by DAVID functional annotation bioinformatics microarray analysis <https://david.ncifcrf.gov> (23). *De novo* motif analyses were also performed with HOMER.

Cross-linking immunoprecipitation of transcribing RNA Pol II

Cross-linking immunoprecipitation with anti-H3K4me3 was performed according to the manufacturer's protocol. Briefly, animals were collected in phosphate buffered saline (PBS) buffer followed by 15 min fixation in 0.75% formaldehyde solution. About 125 mM glycine was added to quench the fixation and animals were transferred to lysis buffer and subjected to sonication to obtain a DNA fragment size of 600–1600 bp. Debris was removed by centrifugation at 8000 *g*. DNA concentration was estimated by measuring absorbance at 260 nm, in order to adjust and obtain the same amount of material for the subsequent immunoprecipitations. About 1.5 μ g of anti-H3K4me3 antibody and 20 μ l of protein A beads were incubated with each sample overnight at 4°C. Protein A beads were then collected and washed three times with wash buffer. 2 \times protein loading buffer was added to the beads and boiled for 3 min to elute the binding DNA–protein complexes. The elution was collected by centrifugation and subjected to western analysis using anti-Pol II S2.

4sU labeling

L1 hatchlings were maintained for 3 days in sterile M9 buffer without bacteria and transferred to NGM plates and fed until the F₂ generation. F₂ adult hermaphrodites were harvested and washed with M9, transferred to new plates with food containing 4sU of the concentrations shown and treated for indicated periods before collection. Total RNA was isolated with TRIzol™ Reagent (Invitrogen) and purified with MaXtract High-Density tubes (Qiagen). Thiol-specific biotinylation and isolation using streptavidin beads was carried out as described previously (24).

Visualization of superimposed track heat maps

EaSeq software (25) was used for visualization to generate superimposed track heat maps as previously described (26). The .bam files were imported using default settings and all values were normalized to reads per kilobase million (RPKM). Line tracks of the superimposed signal were generated using the 'LineTrack' tool, and 1000 bp surrounding each region was segmented into 400 bins and smoothed for 1 bin. Heat maps were made by the 'HeatMap' tool. The 'Colocalize' tool was used to determine the distances from and orientation of each TSS to the nearest peak center. Heat maps were ordered according to increasing size using the 'Sort' tool.

RAD-51 and RNH-1 overexpression lines

Germline expression of *rad-51* or *rnh-1* was driven by a *pie-1* promoter assembled into complex arrays (27). Genomic *rad-51* and *rnh-1.0* were amplified and cloned into pBlue-script vector by Gibson assembly. Primers used for PCR are as follows: *rad-51* (forward: 5'-ATGGGACAATCTTGGG GATATGAAG-3', reverse: 5'-CTAGTCCTCGCGTGCG TCCT-3') and *rnh-1* (forward: 5'-ATGAGCAAGTTCTA TGGTGTGG-3', 5'-TCAAAATCTGAAATTTTTCAAG TTTTGAGT-3'). The *pie-1* promoter and the *pie-1* 3' UTR were used to drive germline expression throughout development. Transgenic lines were generated by microinjecting constructs at 1ng/ μ l as a complex array with *rol-6* marker.

Drug treatments

CHX treatment of L1 larvae during starvation was performed as described previously with 5,6-dichloro-1- β -D-ribofuranosylbenzimidazole (DRB) (2). Briefly, WT and *aak-1/2* L1 larvae obtained by alkaline hypochlorite treatment were maintained in M9 buffer without or with 20 μ M CHX during the 3-day period of diapause. Following this period, L1 larvae were transferred to OP50-seeded NGM plates. When they reached the L4 stage, 50 larvae per condition were isolated, and after 3 days, their fertility and brood size were assessed. Experiments were performed at least thrice. HU and MMS treatments were performed according to previous descriptions (28). For HU treatment, the synchronized L1 larvae without or with 3-day starvation in M9 buffer were transferred to OP50-seeded NGM plates containing HU of indicated concentration and treated for 48 h before being singled into a plate for scoring the fertility. MMS treatment was done similarly to HU treatment except that MMS was added to the M9 buffer at the indicated concentration and treated for the last 12 h of the 3-day starvation.

S9.6 and RAD-51 immunofluorescence

S9.6 immunofluorescence was performed as previously described (29) using secondary antibodies conjugated with Alexa 594. Immunofluorescence analysis of RAD-51 was performed as previously described (30) using secondary antibodies conjugated with Alexa 488. Immunofluorescence images were acquired and processed using a Leica DMI 6000B inverted microscope equipped with a Quorum

WaveFX spinning Disc and EMCCD camera. S9.6 signal intensity and quantification of RAD-51 foci were analyzed and processed with ImageJ software. For quantification of RAD-51 foci, images of the gonads were separated into six equal zones by equally dividing the number of cell rows from the distal end of the gonad to the onset of diakinesis. More than 100 cells were scored in each experiment.

Live imaging

Animals were placed on a slide with a 3% agarose pad and a drop of 0.2 mM levamisole in the M9 buffer. A coverslip was placed on to the drop and sealed with nail polish. Images were taken using spinning-disk confocal microscopy as described above.

PLA

Proximity ligation assay (PLA) was performed with Duolink In Situ PLA[®] Probe Anti-Rabbit PLUS (DUO92002, Sigma-Aldrich), Duolink In Situ PLA[®] Probe Anti-Mouse MINUS (DUO92004, Sigma-Aldrich) and Duolink In Situ Detection Reagents Red (DUO92008, Sigma-Aldrich), according to manufacturer's instructions. The dissected gonads were freeze-cracked with liquid nitrogen before fixation with cold methanol for 10 min. Anti-DNA-RNA hybrid (mouse, 1:50) and anti-RAD-51 (rabbit, 1:1000) antibodies were used.

Statistical analysis

All statistical analyses were performed using GraphPad Prism Software. Error bars indicate standard errors of the mean (S.E.M.) or confidence interval at 95% (95% CI) as indicated. Statistical significance was assessed by Fisher's exact test, Mann-Whitney *U*-test, two-tailed unpaired *t*-test with Welch's correction or one-way ANOVA, as indicated. Statistical significance was considered at $P < 0.05$.

RESULTS

Transgenerational aberrant H3K4me3 deposition occurs predominantly at TSS regions in starved AMPK mutants

The gonads of AMPK mutants recovered from starvation and developed to adulthood are often very disorganized and morphologically abnormal, which is the prominent cause of the sterility observed in the parental generation (P_0). Nevertheless, some of the animals seem to resolve the problems caused by the initial starvation and generate an F_1 brood that appears only mildly or even unaffected. However, in subsequent generations, reproductive defects begin to manifest that become progressively worse with subsequent generations, despite that these later generations of progeny were never starved. The increased abundance of the H3K4me3 sites in the PGCs is propagated to all the germ cells and is maintained over several generations and therefore could be responsible for the transgenerational epigenetic defects in these mutant animals following the acute starvation (2).

To determine how these marks were distributed in the genome and if any suite of affected genes might explain

the sterility and transgenerational epigenetic inheritance, we performed chromatin immunoprecipitation sequencing (ChIP-seq) to generate genome-wide H3K4me3 maps from the F_2 adult descendants of post-L1 diapause (which we refer to hereafter as 'starved') AMPK mutants (31) (Figure 1A). We focused on the F_2 since it is the first generation that is not directly exposed to the starvation (the first transgenerational brood) (31–33). Consistent with our previous findings, H3K4me3 levels are abnormally high in the F_2 descendants of starved AMPK mutants, these 'ectopic' sites of deposition result in a distinct H3K4me3 signature in the starved AMPK mutants (Figure 1B and Supplementary Figure S1A).

H3K4me3 is found primarily on chromatin near or around proximal promoters or TSSs (26). Consistent with this feature, we noted that a high proportion of the 'ectopic' H3K4me3 peaks identified in AMPK mutants were positioned at, or around, promoter regions (Figure 1B–E and Supplementary Figure S1B). Annotation and peak location statistics revealed that the F_2 descendants of starved AMPK mutants harbored more H3K4me3 signals spanning TSSs (Figure 1C, D and Supplementary Figure S1C–E). Further global analysis of H3K4me3 signals indicated that ~88% of the peak calls in the descendants of starved AMPK mutants accumulated at promoter–TSSs, while only ~36% are found at such loci in starved WT animals (Figure 1E).

Blocking the formation of H3K4me3 at TSS–proximal regions is critical for early embryonic development in *C. elegans* (34). We identified that 40% of the total H3K4me3 was deposited at proximal regions (2 kb upstream of TSS) in AMPK mutants compared to only ~24% in WT animals (Supplementary Figure S2A). Moreover, these 'ectopic' sites do not correlate strongly with previously described loci occupied by the nontranscribing paused/poised form of Pol II (35) (Supplementary Figure S2B). This suggests that the 'ectopic' deposition of these H3K4me3 marks could generate an abnormal transcription-activating signal at the TSS–proximal regions of these loci that would otherwise not be earmarked for expression.

If this was indeed the case and the ectopic sites of H3K4me3 were functional, they should be associated with a larger fraction of Pol II that is engaged in transcription. Pol II is phosphorylated by two different kinases, each of which acts at distinct stages of transcription. Serine 5 phosphorylation of the heptapeptide repeats in the Pol II carboxyl terminal domain (S5) occurs after transcription initiation. This form is typically found at the 5' end of genes, where the enzyme pauses prior to promoter clearance. Actively transcribed genes have increased levels of elongating Pol II in the body of the gene that can be distinguished from the post-initiation/poised enzyme (S5) by its characteristic phosphorylation on serine 2 of its carboxyl terminal domain (S2) (12,13). We therefore assessed the levels of the S2-modified form of Pol II in the F_2 descendants of starved WT and AMPK mutants and found that its abundance was higher in the AMPK mutants. The S2-phosphorylated Pol II levels were also enriched in ChIPs of H3K4me3-associated fragments isolated from the AMPK mutants compared to WT animals (Figure 1F). These data are consistent with Pol II being more globally engaged in elongation in starved AMPK mutants, and this is particularly true at the sites of

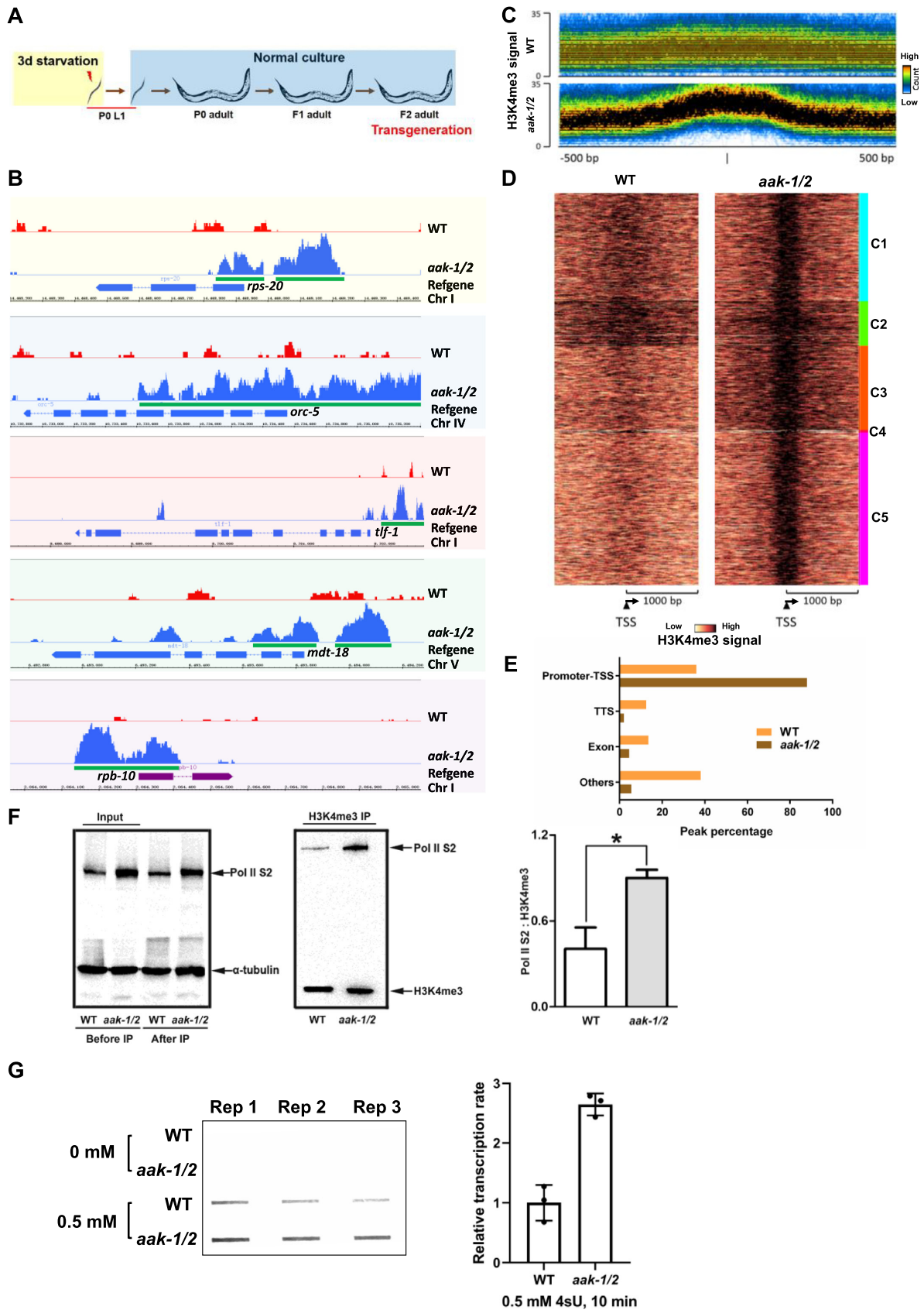


Figure 1. Aberrant H3K4me3 deposition occurs predominantly at TSS regions in starved AMPK mutant descendants. (A) Sample collection scheme for H3K4me3 ChIP-seq analysis. P₀ L1 diapauses were starved for 3 days in M9 buffer, after which larvae were fed until F₂ adult collection. (B)

H3K4me3. However, this analysis cannot distinguish an actively elongating enzyme from Pol II that is stalled in the gene body and no longer actively transcribing. This kind of stalling can occur in genomic regions where the GC content of the template is abnormally high, while also causing additional elongating Pol II complexes to pile up behind the stalled enzyme (12,13).

By performing 4sU run-on assays to monitor the activity of Pol II, we show the direct evidence that in starved AMPK mutants the increased level of Pol II S2 corresponds to complexes that were actively transcribing and not simply paused, or complexes that were piling up behind a stalled enzyme (Figure 1G). This is once again consistent with our previous analyses with the transcription elongation inhibitor, DRB, which showed that blocking transcriptional elongation during the period of quiescence could improve the sterility typical of AMPK mutants (2). Taken together, these data suggest that the ectopically deposited H3K4me3 marks that occur in the AMPK mutant animals are associated with an increased fraction of elongating Pol II, resulting in the inappropriate transcription of a suite of genes in proximity to these histone marks. This unscheduled, premature transcription during the quiescent period of the L1 diapause contributes to the subsequent reproductive defects observed in the recovered mutant animals.

Enhanced R-loop formation within the germ line of starved AMPK mutant descendants

If the accumulation of these transcripts is miscoordinated with their functional requirement during post-embryonic developmental progression, they could negatively impact cellular homeostasis and growth, thus accounting for the numerous defects typically observed in these mutants. To determine if this unscheduled transcription affects the starvation-induced sterility through untimely protein synthesis from the aberrant RNA transcripts, we treated the AMPK mutant L1 larvae with the translation inhibitor CHX during the period of starvation (Supplementary Figure S3), exactly as we had done with DRB. We evaluated sterility following recovery of the starved animals after being transferred to replete growth conditions. Unlike treatment with the transcription inhibitor (2), blocking translation during the L1 diapause did not improve the starvation-induced sterility of the AMPK mutants (Figure 2A). These results strongly suggest that many of the starvation-induced reproductive defects typical of AMPK mutants arise, at least partially, from the inappropriate

transcription/elongation that initially occurs in the PGCs (2), or potentially from the untimely expression or incorrect noncoding RNA products that are generated during the period of acute starvation.

Because elongating Pol II often pauses when not associated with critical factors required for RNA processing and efficient processivity, we wondered if the hyperactivated transcriptional elongation could lead to abnormal R-loop formation in AMPK mutants. R-loops commonly arise at transcriptional pause sites, whereby the nascent pre-mRNA can thread back into the transcription bubble to form an RNA–DNA duplex with the exposed DNA template strand. Using S9.6 antibody that recognizes these structures, we first compared the frequency of R-loops in unstarved WT and AMPK mutant germ lines and found no significant difference (Supplementary Figure S4A). However, we noted that starved AMPK mutant germ lines displayed significantly higher levels of R-loop foci. In parallel, as a positive control, we stained the germ line of a mutant that is deficient for the Tho–Trex complex (*thoc-2*) that results in an increased abundance of R-loops (Figure 2B) (36). The S9.6 signal could be partially alleviated by microinjecting RNaseH (RNH) (37) (Supplementary Figure S4B) or by inhibiting inappropriate transcriptional elongation with DRB during the period of starvation (Supplementary Figure S4C). Moreover, transgenic expression of the *C. elegans* RNH ortholog (*rnh-1*) in the germ cells also improved the fertility of the starved P₀ generation (Figure 2C). Importantly, like the H3K4me3 levels (2), the abnormal abundance of R-loops was gradually resolved over multiple generations, whereby R-loop numbers were most abundant in the germ cells of P₀ adult animals following the initial starvation > F₂ descendants > F₅ descendants (Figure 2D).

R-loop accumulation results from increased H3K4me3

To better understand the relationship between elevated H3K4me3 level and the increased frequency of R-loop formation in AMPK mutants, DRIP-seq were performed using genomic DNA obtained from the F₂ generation of starved WT and AMPK mutant animals (Supplementary Figure S5A). We noted a dramatic expansion in the number of R-loops at loci that had not previously been associated with these structures (36) but also in overall abundance at individual loci throughout the entire genome (Supplementary Figure S5B) of the starved AMPK mutants by comparing both read coverage and depth (Figure 3A and B), with

Genome browser snapshots of H3K4me3 ChIP-seq signals at the promoter–TSS regions of *rps-20*, *orc-5*, *tlf-1*, *mdt-18* and *rpb-10* genes. Green bars show promoter–TSS H3K4me3 calls. Track height represents read counts. (C) Line tracks of H3K4me3 signal at TSSs in WT versus AMPK mutants. Colors indicating H3K4me3 levels are shown on the right. (D) *k*-means clustered heat maps of H3K4me3 signal for WT and *aak-1/2* animals at TSSs. Five different clusters were identified at the 1 kb regions flanking the TSSs, and densities correspond to H3K4me3 signal; C1–C5, clusters 1–5. (E) Annotation and peak location analyses for called H3K4me peaks that map to promoter–TSS, transcription termination site (TTS), exon and the other regions. Peak percentage is shown. In *aak-1/2* mutants, peaks accumulate at the promoter–TSS fraction. (F) Aberrant H3K4me3 sites in starved AMPK mutants are transcriptionally engaged. ChIP was performed with anti-H3K4me3 in both post-L1 diapause WT (N2) and AMPK mutant F₂ adults. The levels of Pol II S2 were first analyzed by western blot using total *C. elegans* lysates immediately following sonication (before IP reaction). A second western blot was performed to ensure that the Pol II S2 was not degraded or dephosphorylated during the IP reaction. The immunoprecipitates were eluted and then immunoblotted with antibodies that recognize Pol II S2 and H3K4me3. The ratio of Pol II S2 to H3K4me3 signal was quantified as indicated in the right panel. The asterisk (*) indicates $P < 0.05$ by Student's *t*-test. (G) Ongoing active transcription is higher in starved AMPK mutants. 4sU labeling was used to assess active transcription in the F₂ descendants of starved AMPK mutant L1 larvae similarly treated WT controls (left panel). Rates of incorporation were assessed after a 10-min pulse and quantified (right panel).

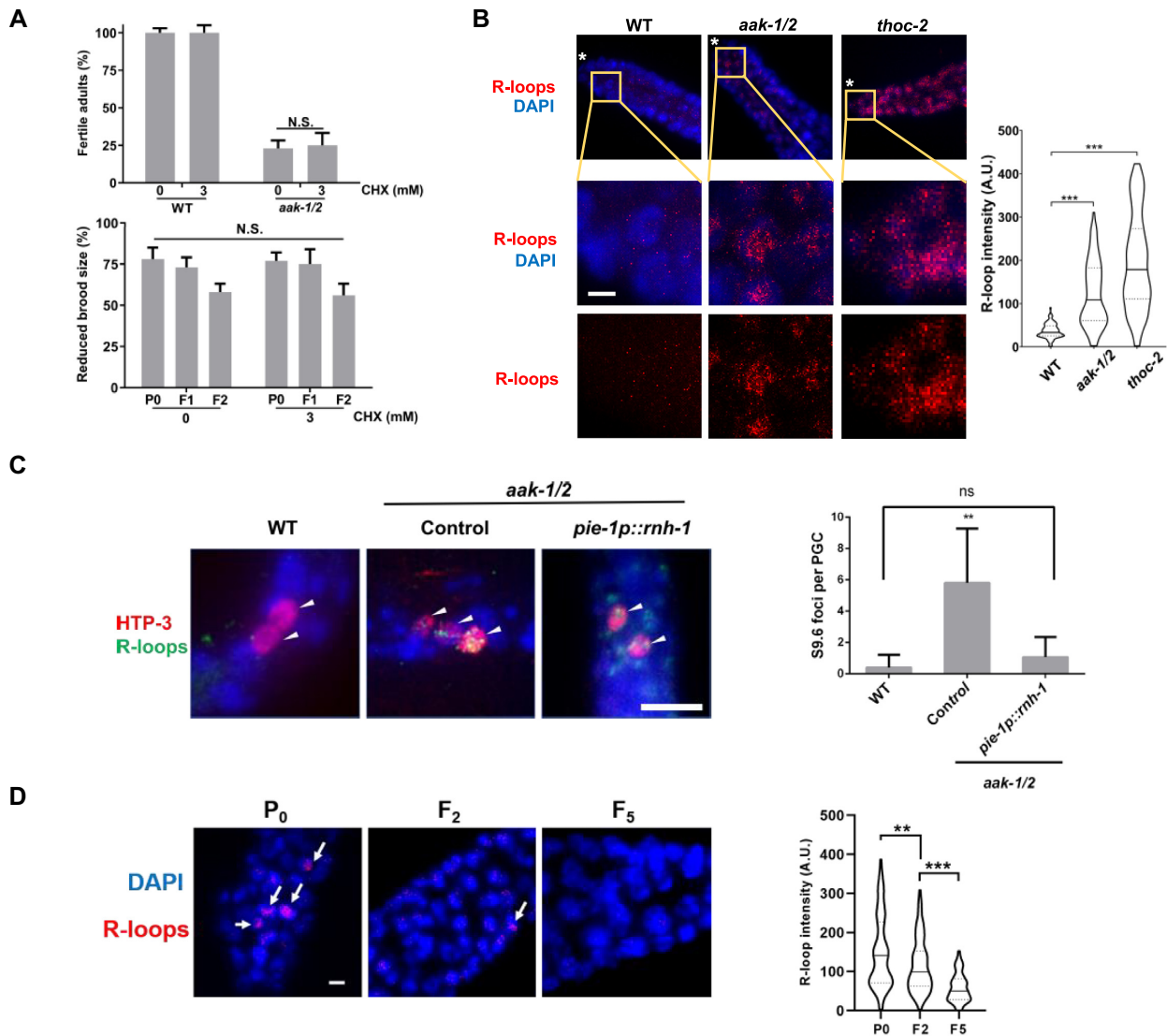


Figure 2. R-loops accumulate within the germ line of starved AMPK mutants. (A) The observed reproductive phenotypes in post-L1 diapause AMPK mutants (P₀) are not caused by untimely protein synthesis. Upper: Emergent WT and *aak-1/2* larvae were maintained in M9 buffer containing CHX of indicated concentrations for 3 days before being transferred to replete plates. The proportion of fertile adult animals is represented, $n \geq 150$. Error bars represent the 95% CI; N.S. by Fisher's exact test. Lower: Transgenerational brood size defects are not restored in the progeny of post-L1 diapause AMPK mutant larvae treated with CHX during the period of starvation. The frequency of animals with reduced brood size in *aak-1/2* mutants and in the subsequent generation (F₁ and F₂) is represented $n \geq 50$. Error bars: 95% CI; N.S. by Fisher's exact test. (B) R-loops accumulate in the germ cells of AMPK mutants. Representative micrographs showing R-loops in young adult germ lines of the starved AMPK mutants and WT. The germ line of a *thoc-2* mutant is shown as a positive control for R-loop detection. Emergent WT and *aak-1/2* L1 larvae were starved 3 days then transferred to replete conditions. Germ lines were fixed and immunostained with S9.6 antibody (R-loops) (red) and counterstained with DAPI (blue). Boxes mark sections that are shown in higher magnification below ($N = 3$, $n = 100$). Asterisk (*) indicates the distal tip cell; scale bar: 5 μm . Right panel: Quantification of nuclear RNA–DNA hybrids in the immunofluorescence demonstrated a clear increase in overall R-loop abundance in the germ lines of starved AMPK mutants; $n = 100$, $***P < 0.001$ by one-way ANOVA, mean \pm S.E.M. (C) R-loops form in the PGCs during the period of starvation in AMPK mutants and are resolved following expression of RNH-1. Emergent WT and *aak-1/2* L1 larvae were starved 3 days then immunostained with S9.6 antibody (R-loops-green) and counterstained with the germ cell specific marker HIM-3 Paralog (HTP-3) (red). Similar starved mutant animals expressing a germline-specific RNH-1 transgene (*pie-1p::rnh-1*) possessed R-loop levels similar to controls. R-loop levels in the PGCs of each genotype were quantified and shown graphically below. White arrowheads indicate PGCs (note that starved AMPK mutants possess additional PGCs); scale bar: 5 μm , $n = 25$, $**P < 0.01$ according to ANOVA with multiple comparisons. (D) R-loops are progressively resolved with successive generations in AMPK mutants. Representative images of DNA–RNA hybrids in the nuclei of P₀ ($n = 83$), F₂ ($n = 100$) and F₅ ($n = 81$) adult germ lines determined by immunofluorescence using the S9.6 antibody (R-loops-red) and counterstained with DAPI (blue). White arrows indicate R-loop (S9.6) foci. P₀ ($n = 83$), F₂ ($n = 100$) and F₅ ($n = 81$) were analyzed by immunofluorescence using the S9.6 antibody. Representative images are shown; scale bars: 5 μm , $N = 2$; $**P < 0.01$, $***P < 0.001$ by Mann–Whitney test.

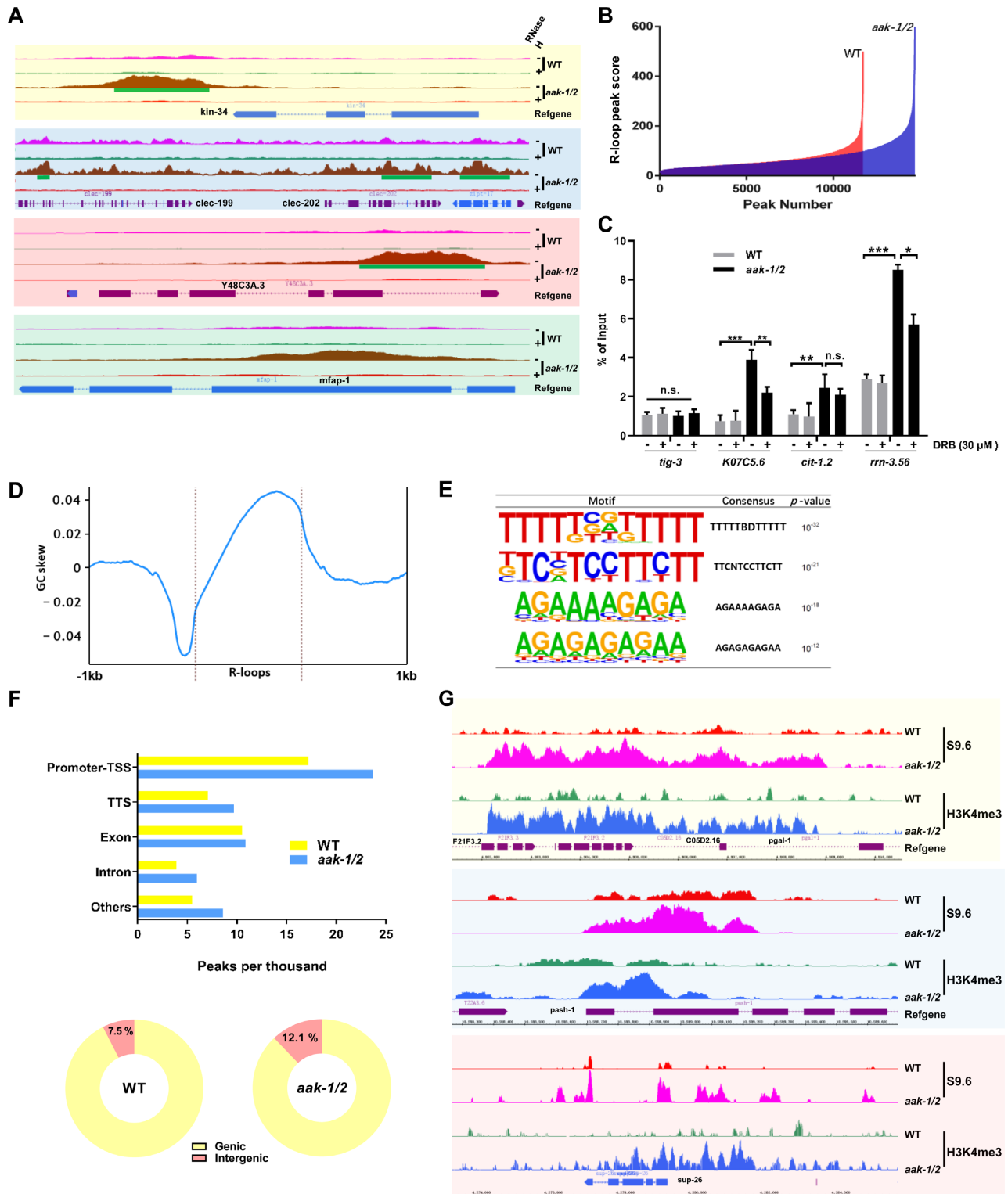


Figure 3. R-loop formation correlates with ectopic deposition of H3K4me3. (A) Genome browser snapshots of DRIP-seq signals at regions proximal to genes and RNase tracks. Green bars show R-loop peak calls. Track height represents read counts. (B) Overall comparison of DRIP-seq output (peak score and number) in WT versus *aak-1/2* genome. (C) DRIP-qPCR validation. WT or F₂ descendants of starved *aak-1/2* mutants cultured with or without DRB treatment during starvation for 3 days were collected for DRIP. *tig-3* was selected as a negative control; $n = 3$, mean \pm S.E.M. Signal values normalized with respect to input genomic DNA are plotted. * $P < 0.05$, ** $P < 0.01$, *** $P < 0.001$ by Mann-Whitney *U*-test. (D) Metaplot of GC skew centered on all R-loop peaks. (E) Four enriched *de novo* motifs identified by HOMER analysis of AMPK mutant versus WT DRIP-seq. (F) Upper: annotation and peak location analyses for called R-loop peaks mapping to promoter-TSS, TTS, exon, intron and the other regions. Genomic peak proportion in per thousand is shown. Peaks accumulate predominantly at the promoter-TSS fraction in *aak-1/2* mutants. Lower: pie charts of DRIP-seq signal distribution for genic versus intergenic regions in WT or F₂ descendants of starved *aak-1/2* mutants. (G) Genome browser snapshots showing a representative sample of positively correlated R-loop signals and H3K4me3 levels in the F₂ descendants of starved AMPK mutants.

high reproducibility between biological replicates (Supplementary Figure S6A,B). The locus-specific enrichment of R-loops was validated by DRIP-qPCR in which about half of the enhanced R-loops in AMPK mutants could be resolved by blocking elongation during the period of starvation (Supplementary Figure S4C), while others remained unchanged (e.g. *cit-1.2*, Figure 3C).

Genome-wide DRIP-seq allowed us to identify a significant proportion of the genome (3.1% and 4.7% in starved WT and AMPK mutants, respectively) that was associated with R-loops in *C. elegans* (Supplementary Figure S6C). A considerable number of the identified R-loop-associated genomic regions were conserved between the both WT and AMPK mutants (Supplementary Figure S6D), suggesting the presence of a common R-loop forming feature in or around these loci (38). Consistent with the report in *Saccharomyces cerevisiae* (39) and human cells (40) that R-loops are not restricted to nuclear genes, we also detect them in the mitochondrial genome of *C. elegans* (Supplementary Figures S5B and S6E). In *Drosophila*, R-loops are highly enriched in repetitive DNA sequences such as satellite DNAs (41). We also observed that a substantial number of R-loops arise within satellite DNA regions, preferentially at centromeric heterochromatin (Supplementary Figure S6F).

GC skew contributes to R-loop formation in humans (14,41). The genomic sequence present within the extracted R-loop peaks from 1 kb up- and downstream exhibit strong GC skew in *C. elegans*, especially in the regions adjacent to the R-loop peaks (Figure 3D). Although AT skew (42) was not revealed in our genome-wide analysis, we did note that there are a substantial number of R-loop-associated sequences with strong AT skew in *C. elegans* (Supplementary Figure S7), especially in starved AMPK mutants (Figure 3E). Two polypyrimidine sequences and two poly(A) tracts were identified by HOMER *de novo* motif analysis (Figure 3E) in AMPK mutant versus WT, suggesting the possibility that a subset of R-loops can form in sequences associated with trans-splicing and/or polyadenylation (38,39).

Genome-wide analyses indicate that overall R-loop intensity in *C. elegans* is most pronounced at the promoter-TSS region (Figure 3F and Supplementary Figure S8A-C). Notably, R-loops that accumulate at the promoter-TSS region occupy ~2.4% of the genome in AMPK mutants, compared to only ~1.7% in WT controls. Besides the promoter-TSS regions, R-loops at transcriptional termination sites (TTSs) occupied ~20% of the total peaks (Figure 3F), which is comparable to estimates of prevalent and conserved R-loop formation at promoter and terminator regions of Pol II-dependent genes in human and mouse genomes (43,44). Among those genes with common promoter-associated R-loops in WT and the F₂ descendants of starved AMPK mutant animals, only a small number of them (~5.6%) also share R-loops at the corresponding TTS regions (Supplementary Figure S8D), suggesting that distinct mechanisms are involved in the regulation of R-loop dynamics at these two intragenic hotspots. The proportion of R-loop peaks in the intron regions was relatively low in both samples (Figure 3F and Supplementary Figure S8A, B). However, genome-wide R-loop signal distribution was higher throughout intergenic regions in AMPK null animals (Figure 3F), suggesting that AMPK could potentially

regulate R-loop formation by restricting the expression of intergenic sequences (45).

Considering that our H3K4me₃, ChIP-seq and DRIP-seq signals have similar distribution patterns at the promoter-TSS regions in starved AMPK mutants (Figures 1E and 3F) and that genes with promoter-localized R-loops coincide with significantly higher transcription activity of the resident genes (43), our data suggest that the increased abundance of conserved and ectopic H3K4me₃ deposition correlates with the formation and/or maintenance of R-loops in AMPK mutants (Figure 3G and Supplementary Figure S8E). We characterized 110 genes with both ectopic R-loops and H3K4me₃ marks (Supplementary Table S2) using the Enrichment Analysis tool from wormbase.org and found that the majority of these genes are indeed expressed in the germ line and the reproductive system (Supplementary Figure S9A), which is consistent with the sterile phenotype that is typical of these animals.

We reported previously that PGCs of starved AMPK mutant L1 larvae have abnormally high levels of nuclear localized SET-2. The COMPASS-like SET-2 histone methyltransferase complex is targeted by AMPK during the L1 diapause, thereby preventing nuclear localization of the complex and corresponding increases in H3K4me₃ in the germ line (2). The association between aberrant H3K4me₃ and R-loop formation was further supported by the RNA interference (RNAi) compromise of the SET-2 histone methyltransferase. *set-2* RNAi results in a significant suppression of R-loop abundance (Supplementary Figure S9B), indicating once more that the R-loops arise from the aberrant H3K4me₃ deposition that occurs during the L1 diapause in the absence of AMPK regulation. Moreover, the converse is not true: the H3K4me₃ levels were not affected by the reduction in R-loop abundance in the *rmh-1*-expressing animals (Supplementary Figure S9C).

Abnormal recruitment of RAD-51 to R-loop-associated loci

Persistent, unresolved R-loops have been shown to promote DNA damage and genomic instability (41,46). In yeast, elevated R-loop levels strongly correlate with sites of replication stress-induced DNA damage (47). We noted that both the AMPK mutants and the F₂ descendants of starved AMPK mutant animals were hypersensitive to HU and the alkylating agent MMS, both of which are genotoxic drugs that compromise DNA replication (48) (Figure 4A and Supplementary Figure S10). These findings implicate AMPK function in the normal DNA repair process that occurs in response to genotoxic insult. However, the effects of its absence are exacerbated following starvation, as AMPK mutants are hypersensitive to DNA damage and/or replication stress, potentially due to the increased abundance of R-loops.

RAD-51 plays a critical role in the recognition of damage sites and their eventual repair (49,50). During meiosis, the DSBs typical of meiotic intermediates are also recognized and bound by RAD-51 in the *C. elegans* germ cells (51,52). We observed comparatively more RAD-51 foci (markers of DSB repair intermediates) in the germ lines of starved AMPK mutants, and this is observed at each stage of meiotic prophase (Figure 4B and C). The RAD-51 recruit-

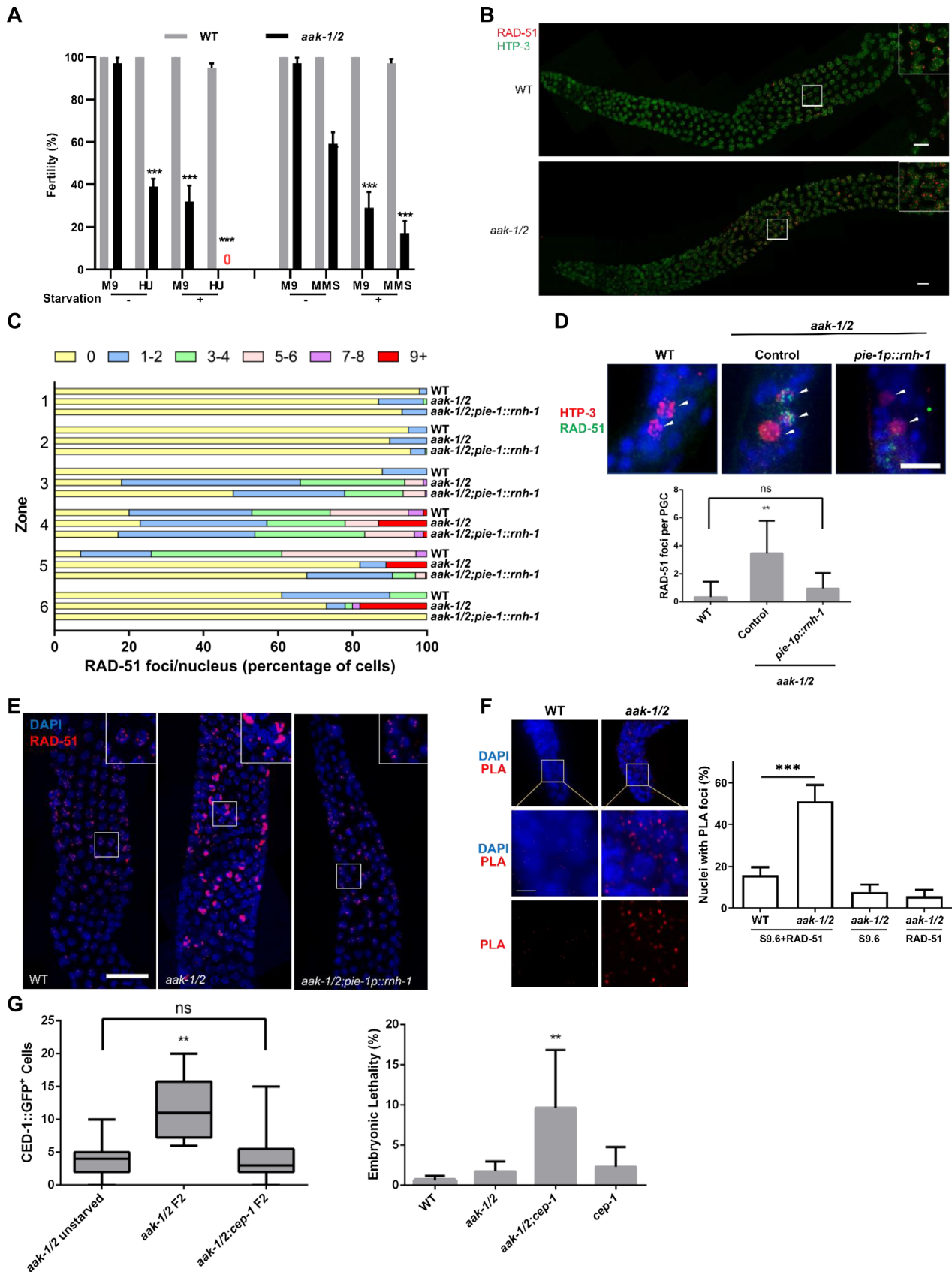


Figure 4. Starvation results in the abnormal recruitment of RAD-51 to R-loop associated loci in AMPK mutants. (A) AMPK mutant L1 larvae are sensitive to genotoxic stress and become hypersensitive following starvation. L1 larvae that were starved or fed for 4 h were subjected to 25 mM HU and 0.01%

ment already occurs during the period of starvation in the PGCs of the AMPK mutant L1 larvae and is entirely dependent on the formation of R-loops, as it is suppressed by RNH-1 expression (Figure 4D). The situation is similar in the adult germ line, where the RAD-51 aggregates that form in starved AMPK mutants are also eliminated by the expression of additional copies of RNH-1 specifically in the germ line (Figure 4E). This suggests that the recruitment and abnormal accumulation of RAD-51 in the germ cells of AMPK mutants is associated with the abnormal R-loop formation, potentially on the accessible single-stranded DNA present in these structures or at sites of DNA damage that arise due to their presence.

To address the possibility that RAD-51 might be accumulating at loci associated with R-loops, we determined the physical overlap between RNA-DNA hybrids and RAD-51 in the germ lines of the descendants of starved AMPK mutants using a PLA that detects interactions to a limit 30–40 nm (53). Indeed, RAD-51 is localized to R-loops at a subset of these supernumerary RAD-51 foci, while positive PLA signals were nearly undetectable in starved WT germ lines (Figure 4F). This indicates that DNA damage is induced at these R-loops, potentially due to transcription–replication conflicts that arise in the mitotic zone and persist, or alternatively, it may represent collateral sites of damage that arise during the process of R-loop resolution or interference with normal meiotic progression (54). Moreover, we noticed that nuclei with highly abundant RAD-51 foci often appeared in the pachytene region of the germ line of AMPK mutants (Figure 4B and C), suggesting that these nuclei may have irreparable damage and could be destined for elimination (55). The membrane bound phagocytic receptor CED-1 surrounds apoptotic cells undergoing corpse engulfment and therefore is an excellent proxy to quantify cells undergoing the final steps of apoptosis (36). We observed an increased number of CED-1::GFP positive cells indicating that the frequency of apoptotic cell death (36) was significantly enhanced in the germ lines of starved AMPK mutants (Figure 4G).

If these germline cell deaths are triggered by excess irreparable DNA damage incurred in these post-starvation AMPK mutants, the *C. elegans* p53 ortholog *cep-1* should become activated to specify their elimination (56,57). We

thus quantified the frequency of germ cells expressing CED-1::GFP in the starved mutant animals that lack *cep-1* function. Our analysis indicated that the levels of CED-1::GFP were suppressed in the AMPK mutant animals that lack *cep-1/p53* function, consistent with a requirement for p53-mediated signaling to trigger germline apoptosis in response to increased R-loop formation and subsequent RAD-51 aggregation (Figure 4G). Furthermore, if the cells that were not culled due to the lack of *cep-1* were permitted to contribute to the F₁ brood by eliminating the critical cell death effector *ced-3*, we noted that embryonic lethality was consequently increased in the AMPK mutants that lacked *cep-1* function (Figure 4G). These data suggest that in these mutant animals, the germ cells that would normally have been culled in a p53-dependent manner, instead progress through oogenesis to eventually generate embryos that die in the early stages of development, presumably due to an accumulation of excessive unrepaired damage.

RAD-51 sequestration at R-loop loci limits its availability during meiosis, resulting in starvation-dependent sterility

If RAD-51 is sequestered at these sites, it could potentially limit its normal involvement in the resolution of double-strand break that occurs during meiosis, thereby contributing to the sterility observed in the AMPK mutant adults that were previously starved as larvae. To determine if RAD-51 function is limiting in the germ line due to its sequestration at R-loops, we expressed additional copies of RAD-51 in the germ cells of AMPK mutants. The sterility of the affected P₀ animals is most likely a result of both defects in somatic gonad development and germ cell integrity, thus resulting in a highly disorganized gonad with almost no surviving F₁ progeny. However, by providing a surplus of RAD-51, driven by a germ-cell specific promoter, partially suppressed the sterility of previously starved AMPK mutant P₀ hermaphrodites to a degree that was comparable to that observed when RNH-1 was expressed in the germ line using the same promoter (Figure 5A).

Taken together, these data suggest that *C. elegans* larvae that lack AMPK signaling ectopically deposit H3K4me3 marks in the PGCs during the L1 diapause. These modifications trigger unscheduled transcriptional elongation that is

MMS at sub-threshold concentrations previously determined to cause sterility in WT animals (48); mean \pm S.E.M, *** $P < 0.001$ by unpaired *t*-test with Welch's correction. Each assay was independently performed at least thrice. (B) RAD-51 foci are abnormally increased in the germ lines of starved AMPK mutants. Gonads were stained with RAD-51 antibody (red) and counterstained with HTP-3 (green). White framed regions are shown in high magnification in the insets; scale bar: 10 μ m. (C) Quantification of number and time of appearance of RAD-51 foci in six zones of the germ line: mitotic, transition zone, early pachytene, mid-pachytene, late pachytene and diplotene, $n > 5$. (D) Representative micrographs showing RAD-51 foci in the PGCs of 3-day starved L1 larvae. Whole larvae were collected and immunostained with RAD-51 antibody (green) and counterstained with HTP-3 (red). Arrowheads indicate PGCs (note that starved AMPK mutants possess additional PGCs); scale bar: 5 μ m. (E) Immunofluorescence micrographs showing RAD-51 foci in the late pachytene region of young adult germ lines of starved WT, *aak-1/2* mutants and *aak-1/2; pie-1p::rnh-1*. Gonads were immunostained with RAD-51 antibody (red) and counterstained with DAPI (blue). White framed regions are shown in higher magnification in insets; scale bar: 10 μ m. (F) Abnormally abundant RAD-51 signals overlap with R-loops in the germ cells of F₂ descendants of previously starved AMPK mutants. Upper: PLA signals are indicated by red spots. Asterisk (*) indicates the distal tip cell. Framed regions in each merged micrograph are shown in higher magnification directly below for each genotype; scale bar: 5 μ m. Lower: Quantification of the percentage of nuclei with PLA foci per germ line. Single-antibody controls from AMPK mutant germ lines are shown; $n = 5$. *** $P < 0.001$ by Student's *t*-test, mean \pm S.E.M. (G) Left: The increased cell death in the gonads of starved WT versus AMPK mutants is DNA damage dependent. Apoptotic bodies were quantified by counting Cell Death Abnormal (CED)-1::GFP positive cells in the gonad arms. Boxplots show average, boxes 50% and whiskers min to max of the group, $n = 25$. ** $P < 0.01$ by ANOVA with multiple comparisons test. Right: Removal of *cep-1* signaling increases embryonic lethality in the gonads of starved WT versus AMPK mutants. Quantification of embryonic lethality among the F₂ descendants of the previously starved animals of indicated genotype. Individuals scored: WT, $n = 10$, *aak-1(tm1844)* I, *aak-2(ok524)* X, $n = 10$, *aak-1(tm1844)* I, *aak-2(ok524)* X; *cep-1(gk138)* I, $n = 20$, *cep-1(gk138)* I, $n = 20$. Bar graph shows group average with SD and assessed by ANOVA with multiple comparisons tests; ** $P < 0.01$.

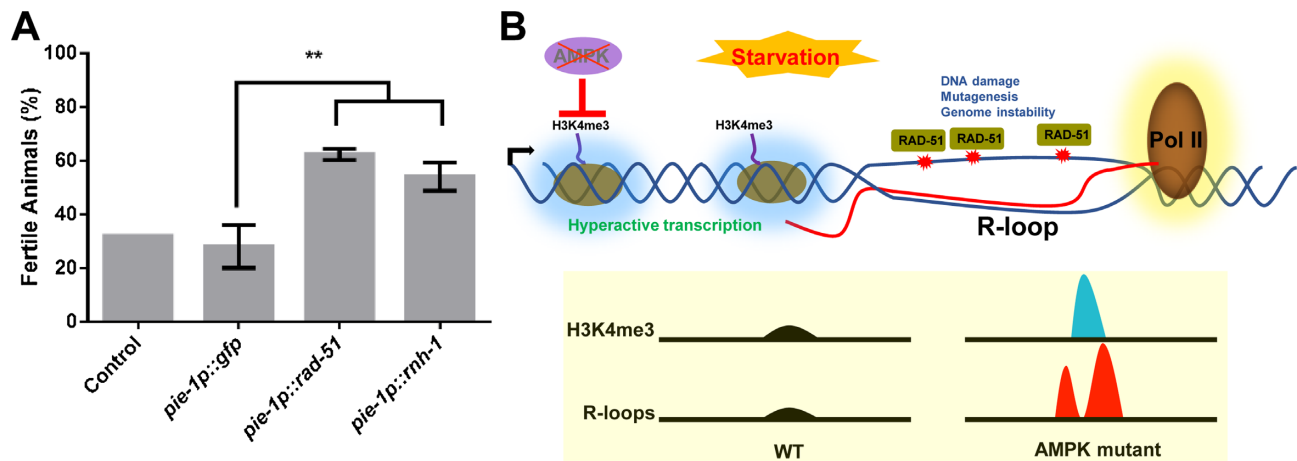


Figure 5. RAD-51 sequestration at R-loop sites limits its availability during meiosis, resulting in starvation-dependent sterility. (A) Multicopy arrays of *pie-1p::rad-51* can partially restore poststarvation fertility in AMPK mutants. Transgenic L1 larvae were maintained in M9 buffer for 72 h at 20°C. Animals were then recovered to replete conditions. The percent fertility was assessed 96 h following recovery. Error bars represent the SD. $**P < 0.01$ when compared to controls using unpaired *t*-test, $n = 25$. (B) Model depicting AMPK-dependent events that occur during acute starvation. AMPK constrains inappropriate H3K4me3 deposition and consequent transcription that causes increases R-loop formation and genomic instability.

associated with a consequent increased frequency of R-loop formation. These hybrid structures are transmissible owing to their association with their corresponding H3K4me3 marks. This failure in AMPK-dependent epigenetic regulation could therefore account for the inheritable abnormalities in reproductive development, DNA damage hypersensitivity, enhanced germline apoptosis and the sterility that is typical of the post-L1 diapause AMPK mutants (Figure 5B).

DISCUSSION

The importance of developmental quiescence is most clearly revealed in the phenotypes that arise following its untimely reversal (2,58–62). When first stage *C. elegans* larvae are subjected to acute starvation, there are very few, if any, consequences that persist following recovery, although this changes with more chronic starvation (6). This resilience is largely dependent on the efficient activity of AMPK to reallocate resources and protect both the individual cells, most importantly the germ cells, and the organism as a whole. As we have previously shown, animals that lack AMPK signaling abnormally undergo supernumerary germ cell divisions during the period of starvation. This ‘escape’ from quiescence is accompanied by both short- and long-term (transgenerational) consequences, many of which arise due to inappropriate SET1/MLL-dependent chromatin modifications in the germ cells that occur during a relatively short period when the animals should normally be in quiescent state. This is by no means unique to *C. elegans*; the misregulated gene expression associated with aberrant SET1/MLL activity has been associated with various types of cancer and/or inappropriate developmental outcomes (63).

Using *C. elegans* as a model, we showed that the protein kinase AMPK links physiological and/or metabolic status to adaptive changes in gene regulation that are critical for adjustment during periods of duress. During the L1 diapause, this is mediated in part by regulating the nuclear accumulation of the MLL ortholog SET-2, an important his-

tone methyltransferase enzyme associated with earmarking chromatin for transcriptional activation.

The loss of AMPK during the diapause results in premature lethality, but this can be reversed following feeding in the first few days. Although the reason for the premature lethality seen in starved AMPK mutant L1 larvae remains unclear, the surviving animals that recover following transfer to sufficient growth conditions grow to become sterile adults, and this sterility is partially due to the inappropriate regulation of SET-2. Curiously, the sterility observed in the P_0 could be partially reversed by blocking transcriptional elongation but not by inhibiting protein synthesis. Therefore, at least part of the sterility that occurs in these mutant adults must result from the process of transcription per se or the RNA products that arise from these events.

We noted that the increase in the SET-2-dependent H3K4me3 marks that accumulate in starved AMPK mutants results in a consequent increase in R-loop formation, presumably due to the premature activation of Pol II complexes. If Pol II stalls, the nascent pre-mRNA may then thread back to form R-loops at these sites, increasing the risk of DSB formation due to replication/transcription conflicts or simply the sequestration of key players in the DNA damage response such as RAD-51.

Although we have determined that the aberrant R-loop formation in starved AMPK mutants is intimately linked to the resultant transcription that occurs at many of these ectopic H3K4me3 sites, it remains unclear what distinguishes where the SET-2/COMPASS-like complex will deposit these ectopic H3K4me3 sites in the PGCs of starved mutant animals. Our sequence analysis of the genes that become marked in starved mutants did not reveal any apparent common signature that would suggest some functional or adaptive rationale that dictates the location of this deposition. The entire process may occur as the result of a population of residual small RNAs that recruit the methyltransferase complex to the incorrect loci. This would not occur in animals that possess active AMPK, since the enzyme would be excluded from the nucleus. In WT, these RNAs might

be eliminated as post-embryonic development is triggered with feeding, allowing the SET-2/COMPASS-like complex to access the chromatin in order to couple the necessary epigenetic changes and consequent gene expression program with larval growth and development.

The same question is relevant for the R-loops. Why are some H3K4me3 modified loci associated with increased R-loop formation, while others are not? Is there some molecular feature(s) that predisposes a given H3K4me3-marked locus to form an R-loop beyond simply the GC sequence content that is typical of most endogenous R-loops? Once again, our analysis did not reveal any common feature that appears to be shared among the various loci that are associated with these ectopic R-loops. It is possible that the formation and the overall abundance of these R-loops may depend on the various protein components that are bound to these H3K4me3-marked TSSs, which ultimately affect Pol II elongation and/or its processivity (64). In a recent study where R-loop formation was enhanced by the genetic removal of RNH activity, R-loops result in irreparable DNA damage and activation of a damage-sensitive checkpoint. This too seems to be very context dependent where the excess presence of R-loops only triggers apoptosis when they occur in specific genes/loci (55).

Nevertheless, the relationship between the aberrant chromatin marks, the formation of the R-loops, the RAD-51 sequestration and impaired DNA damage response that we describe here may be relevant in other contexts where the deposition of such important epigenetic marks is misregulated. This may be particularly important in cases where the MLL family of histone methyltransferases have been implicated in the etiology of various forms of cancer (65).

The H3K4me3 sites and the associated R-loops first appear during the period of starvation. The R-loops either are not resolved and persist into the adult germ line or are constantly reformed in the germ cell daughters during the ensuing cell divisions. Curiously, from their initial formation until their abundance peaks in the adult germ line, the R-loops are bound by RAD-51. The association of RAD-51 with the 'ectopic' R-loops may compromise its normal function during the early stages of the L1 stage and/or later during meiosis. The initiation of postembryonic development is associated with a rapid increase in gene expression that, like in other organisms, occurs with a concomitant increase in DNA damage, including DSBs and ensuing RAD-51 intervention (66–68). Similarly, during meiosis, RAD-51 is required to bind to recombination intermediates to stabilize and protect these structures during strand invasion and resection. If RAD-51 is stably bound to R-loops, it may be limiting for its function in resolving the DSBs that arise in both cases, resulting in soma/germ line developmental asynchrony in one case and meiotic failure in the other. Both of these scenarios are consistent with the somatic and germline phenotypes we observe in AMPK mutants.

Beyond the apparent reproductive phenotypes that arise in the P₀ and the F₂ generations, the possibility that these aberrant R-loops could result in long-term genetic change cannot be excluded (55). Although the increased frequency of R-loops in starved AMPK mutants is resolved in five generations, the consequences of these mutagenic structures may persist for much longer. During the period that the triplex remains unresolved, the coding strand is highly

vulnerable to sequence-altering enzymes. These modifications are among the most common mutations detected in a wide array of cancer types (69), suggesting that these enzymes are both prevalent and highly active. Any resultant nucleotide substitution can potentially become fixed, giving rise to a permanent genetic change that persists long after the R-loop has been resolved. This may also account for some of the observed spontaneous phenotypes that arise in later generation AMPK mutants that were previously starved, or in the late generation *spr-5* mutants, which have a genome-wide increase in H3K4me2, another transcription-activating chromatin mark that arises due to the lack an Lysine-specific demethylase 1 (LSD1)-like histone demethylase (5).

The genome instability and compromised germline integrity that arises in AMPK mutants due to the increased R-loop frequency is almost certainly not adaptive. On the other hand, it does generate a previously unexpected source of genetic diversity that arises during an otherwise desperate, yet evolutionarily relevant challenge, that being starvation. The maladaptive consequences of these starvation-induced epigenetic modifications may nevertheless presage genetic change or even enhance genetic diversity in these compromised animals (70). The R-loops that form in this context may represent a similar double-edged sword by providing animals with an increased rate of genetic change that is nevertheless accompanied by a corresponding fitness trade-off.

DATA AVAILABILITY

Source data are provided with this paper. These datasets are available under BioProject accession number PR-JNA721008.

SUPPLEMENTARY DATA

Supplementary Data are available at NAR Online.

ACKNOWLEDGEMENTS

The authors are grateful to members of the Roy and Zetka laboratories for reagents, discussion and advice. We are especially grateful to Shaolin Li for discussion and technical assistance with the Pol II immunoprecipitations. Some of the *C. elegans* strains used in this work were provided by the Caenorhabditis Genetics Center (University of Minnesota), which is funded by the NIH National Center for Research Resources (NCR).

Author contributions: B.S. and R.R. planned the study, designed the experiments and wrote the manuscript with input from all coauthors. B.S. and M.S. performed the experiments. B.S. analyzed the data. R.R. supervised the work.

FUNDING

Canadian Institutes for Health Research (CIHR); Grant number PJT-169154. Funding for open access charge: CIHR.

Conflict of interest statement. None declared.

REFERENCES

- Hardie,D.G., Ross,F.A. and Hawley,S.A. (2012) AMPK: a nutrient and energy sensor that maintains energy homeostasis. *Nat. Rev. Mol. Cell Biol.*, **13**, 251–262.
- Demoinet,E., Li,S. and Roy,R. (2017) AMPK blocks starvation-inducible transgenerational defects in *Caenorhabditis elegans*. *Proc. Natl Acad. Sci. USA*, **114**, E2689–E2698.
- Lee,H., Zandkarimi,F., Zhang,Y., Meena,J.K., Kim,J., Zhuang,L., Tyagi,S., Ma,L., Westbrook,T.F., Steinberg,G.R. *et al.* (2020) Energy-stress-mediated AMPK activation inhibits ferroptosis. *Nat. Cell Biol.*, **22**, 225–234.
- Greer,E.L., Becker,B., Latza,C., Antebi,A. and Shi,Y. (2016) Mutation of *C. elegans* demethylase spr-5 extends transgenerational longevity. *Cell Res.*, **26**, 229–238.
- Katz,D.J., Edwards,T.M., Reinke,V. and Kelly,W.G. (2009) A *C. elegans* LSD1 demethylase contributes to germline immortality by reprogramming epigenetic memory. *Cell*, **137**, 308–320.
- Jobson,M.A., Jordan,J.M., Sandrof,M.A., Hibshman,J.D., Lennox,A.L. and Baugh,L.R. (2015) Transgenerational effects of early life starvation on growth, reproduction, and stress resistance in *Caenorhabditis elegans*. *Genetics*, **201**, 201–212.
- Harvey,Z.H., Chakravarty,A.K., Futia,R.A. and Jarosz,D.F. (2020) A prion epigenetic switch establishes an active chromatin state. *Cell*, **180**, 928–940.
- Borg,M., Jacob,Y., Susaki,D., LeBlanc,C., Buendia,D., Axelsson,E., Kawashima,T., Voigt,P., Boavida,L., Becker,J. *et al.* (2020) Targeted reprogramming of H3K27me3 resets epigenetic memory in plant paternal chromatin. *Nat. Cell Biol.*, **22**, 621–629.
- Barucci,G., Cornes,E., Singh,M., Li,B., Ugolini,M., Samolygo,A., Didier,C., Dingli,F., Loew,D., Quarato,P. *et al.* (2020) Small-RNA-mediated transgenerational silencing of histone genes impairs fertility in piRNA mutants. *Nat. Cell Biol.*, **22**, 235–245.
- Fanucchi,S., Fok,E.T., Dalla,E., Shibayama,Y., Borner,K., Chang,E.Y., Stoychev,S., Imakaev,M., Grimm,D., Wang,K.C. *et al.* (2019) Immune genes are primed for robust transcription by proximal long noncoding RNAs located in nuclear compartments. *Nat. Genet.*, **51**, 138–150.
- Skourti-Stathaki,K., Torlai Triglia,E., Warburton,M., Voigt,P., Bird,A. and Pombo,A. (2019) R-Loops enhance polycomb repression at a subset of developmental regulator genes. *Mol. Cell*, **73**, 930–945.
- Ni,Z., Schwartz,B.E., Werner,J., Suarez,J.R. and Lis,J.T. (2004) Coordination of transcription, RNA processing, and surveillance by P-TEFb kinase on heat shock genes. *Mol. Cell*, **13**, 55–65.
- Ni,Z., Saunders,A., Fuda,N.J., Yao,J., Suarez,J.R., Webb,W.W. and Lis,J.T. (2008) P-TEFb is critical for the maturation of RNA polymerase II into productive elongation *in vivo*. *Mol. Cell Biol.*, **28**, 1161–1170.
- Manzo,S.G., Hartono,S.R., Sanz,L.A., Marinello,J., De Biasi,S., Cossarizza,A., Capranico,G. and Chedin,F. (2018) DNA topoisomerase I differentially modulates R-loops across the human genome. *Genome Biol.*, **19**, 100.
- Buisson,R., Langenbucher,A., Bowen,D., Kwan,E.E., Benes,C.H., Zou,L. and Lawrence,M.S. (2019) Passenger hotspot mutations in cancer driven by APOBEC3A and mesoscale genomic features. *Science*, **364**, aaw2872.
- Matos,D.A., Zhang,J.M., Ouyang,J., Nguyen,H.D., Genois,M.M. and Zou,L. (2020) ATR protects the genome against r loops through a MUS81-triggered feedback loop. *Mol. Cell*, **77**, 514–527.
- Garcia-Pichardo,D., Canas,J.C., Garcia-Rubio,M.L., Gomez-Gonzalez,B., Rondon,A.G. and Aguilera,A. (2017) Histone mutants separate R loop formation from genome instability induction. *Mol. Cell*, **66**, 597–609.
- Bolger,A.M., Lohse,M. and Usadel,B. (2014) Trimmomatic: a flexible trimmer for illumina sequence data. *Bioinformatics*, **30**, 2114–2120.
- Li,H. and Durbin,R. (2010) Fast and accurate long-read alignment with burrows-wheeler transform. *Bioinformatics*, **26**, 589–595.
- 1000 Genome Project Data Processing Subgroup, Li,H., Handsaker,B., Wysoker,A., Fennell,T., Ruan,J., Homer,N., Marth,G., Abecasis,G. and Durbin,R. (2009) The sequence alignment/map format and SAMtools. *Bioinformatics*, **25**, 2078–2079.
- Heinz,S., Benner,C., Spann,N., Bertolino,E., Lin,Y.C., Laslo,P., Cheng,J.X., Murre,C., Singh,H. and Glass,C.K. (2010) Simple combinations of lineage-determining transcription factors prime cis-regulatory elements required for macrophage and B cell identities. *Mol. Cell*, **38**, 576–589.
- Zhang,Y., Liu,T., Meyer,C.A., Eeckhoutte,J., Johnson,D.S., Bernstein,B.E., Nusbaum,C., Myers,R.M., Brown,M., Li,W. *et al.* (2008) Model-based analysis of chip-Seq (MACS). *Genome Biol.*, **9**, R137.
- Sun,B., Fan,P., Liao,M. and Zhang,Y. (2018) Modeling endophilin-mediated abeta disposal in glioma cells. *Biochim. Biophys. Acta Mol. Cell Res.*, **1865**, 1385–1396.
- Dolken,L., Ruzsics,Z., Radle,B., Friedel,C.C., Zimmer,R., Mages,J., Hoffmann,R., Dickinson,P., Forster,T., Ghazal,P. *et al.* (2008) High-resolution gene expression profiling for simultaneous kinetic parameter analysis of RNA synthesis and decay. *RNA*, **14**, 1959–1972.
- Lerdrup,M., Johansen,J.V., Agrawal-Singh,S. and Hansen,K. (2016) An interactive environment for agile analysis and visualization of chip-sequencing data. *Nat. Struct. Mol. Biol.*, **23**, 349–357.
- Dahl,J.A., Jung,I., Aanes,H., Greggains,G.D., Manaf,A., Lerdrup,M., Li,G., Kuan,S., Li,B., Lee,A.Y. *et al.* (2016) Broad histone H3K4me3 domains in mouse oocytes modulate maternal-to-zygotic transition. *Nature*, **537**, 548–552.
- Kelly,W.G. and Fire,A. (1998) Chromatin silencing and the maintenance of a functional germline in *Caenorhabditis elegans*. *Development*, **125**, 2451–2456.
- Craig,A.L., Moser,S.C., Bailly,A.P. and Gartner,A. (2012) Methods for studying the DNA damage response in the *caenorhabditis elegans* germ line. *Methods Cell Biol.*, **107**, 321–352.
- Salas-Armenteros,I., Perez-Calero,C., Bayona-Feliu,A., Tumini,E., Luna,R. and Aguilera,A. (2017) Human THO-Sin3A interaction reveals new mechanisms to prevent R-loops that cause genome instability. *EMBO J.*, **36**, 3532–3547.
- Girard,C., Roelens,B., Zawadzki,K.A. and Villeneuve,A.M. (2018) Interdependent and separable functions of *Caenorhabditis elegans* MRN-C complex members couple formation and repair of meiotic DSBs. *Proc. Natl Acad. Sci. USA*, **115**, E4443–E4452.
- Camacho,J., Truong,L., Kurt,Z., Chen,Y.W., Morselli,M., Gutierrez,G., Pellegrini,M., Yang,X. and Allard,P. (2018) The memory of environmental chemical exposure in *C. elegans* is dependent on the jumonji demethylases jmjD-2 and jmjD-3/utx-1. *Cell Rep.*, **23**, 2392–2404.
- Skinner,M.K. (2008) What is an epigenetic transgenerational phenotype? F3 or F2. *Reprod. Toxicol.*, **25**, 2–6.
- Palominos,M.F., Verdugo,L., Gabaldon,C., Pollak,B., Ortiz-Severin,J., Varas,M.A., Chavez,F.P. and Calixto,A. (2017) Transgenerational diapause as an avoidance strategy against bacterial pathogens in *Caenorhabditis elegans*. *Mbio*, **8**, mBio.01234-17.
- Kaser-Pebernard,S., Pfefferli,C., Aschinger,C. and Wicky,C. (2016) Fine-tuning of chromatin composition and polycomb recruitment by two Mi2 homologues during *C. elegans* early embryonic development. *Epigenet. Chromatin*, **9**, 39.
- Maxwell,C.S., Kruesi,W.S., Core,L.J., Kurhanewicz,N., Waters,C.T., Lewarch,C.L., Antoshechkin,I., Lis,J.T., Meyer,B.J. and Baugh,L.R. (2014) Pol II docking and pausing at growth and stress genes in *C. elegans*. *Cell Rep.*, **6**, 455–466.
- Zeller,P., Padeken,J., van Schendel,R., Kalck,V., Tijsterman,M. and Gasser,S.M. (2016) Histone H3K9 methylation is dispensable for *caenorhabditis elegans* development but suppresses RNA:DNA hybrid-associated repeat instability. *Nat. Genet.*, **48**, 1385–1395.
- Castellano-Pozo,M., Garcia-Muse,T. and Aguilera,A. (2012) R-loops cause replication impairment and genome instability during meiosis. *EMBO Rep.*, **13**, 923–929.
- Wahba,L., Costantino,L., Tan,F.J., Zimmer,A. and Koshland,D. (2016) S1-DRIP-seq identifies high expression and polyA tracts as major contributors to R-loop formation. *Genes Dev.*, **30**, 1327–1338.
- Briggs,E., Hamilton,G., Crouch,K., Lapsley,C. and McCulloch,R. (2018) Genome-wide mapping reveals conserved and diverged R-loop activities in the unusual genetic landscape of the african trypanosome genome. *Nucleic Acids Res.*, **46**, 11789–11805.
- Silva,S., Camino,L.P. and Aguilera,A. (2018) Human mitochondrial degradosome prevents harmful mitochondrial R loops and mitochondrial genome instability. *Proc. Natl Acad. Sci. USA*, **115**, 11024–11029.
- Bayona-Feliu,A., Casas-Lamesa,A., Reina,O., Bernues,J. and Azorin,F. (2017) Linker histone H1 prevents R-loop accumulation and genome instability in heterochromatin. *Nat. Commun.*, **8**, 283.

42. Xu,W., Xu,H., Li,K., Fan,Y., Liu,Y., Yang,X. and Sun,Q. (2017) The R-loop is a common chromatin feature of the arabidopsis genome. *Nat Plants*, **3**, 704–714.
43. Sanz,L.A., Hartono,S.R., Lim,Y.W., Steyaert,S., Rajpurkar,A., Ginno,P.A., Xu,X. and Chedin,F. (2016) Prevalent, dynamic, and conserved R-Loop structures associate with specific epigenomic signatures in mammals. *Mol. Cell*, **63**, 167–178.
44. Hatchi,E., Goehring,L., Landini,S., Skourti-Stathaki,K., DeConti,D.K., Abderazzaq,F.O., Banerjee,P., Demers,T.M., Wang,Y.E., Quackenbush,J. *et al.* (2021) BRCA1 and RNAi factors promote repair mediated by small RNAs and PALB2-RAD52. *Nature*, **591**, 665–670.
45. Lloyd,J.P., Tsai,Z.T., Sowers,R.P., Panchy,N.L. and Shiu,S.H. (2018) A model-based approach for identifying functional intergenic transcribed regions and noncoding RNAs. *Mol. Biol. Evol.*, **35**, 1422–1436.
46. Costantino,L. and Koshland,D. (2018) Genome-wide map of R-Loop-Induced damage reveals how a subset of R-Loops contributes to genomic instability. *Mol. Cell*, **71**, 487–497.
47. Teloni,F., Michelena,J., Lezaja,A., Kilic,S., Ambrosi,C., Menon,S., Dobrovolna,J., Imhof,R., Janscak,P., Baubec,T. *et al.* (2019) Efficient Pre-mRNA cleavage prevents replication-stress-associated genome instability. *Mol. Cell*, **73**, 670–683.
48. Litwin,I., Bakowski,T., Szakal,B., Pilarczyk,E., Maciaszyk-Dziubinska,E., Branzei,D. and Wysocki,R. (2018) Error-free DNA damage tolerance pathway is facilitated by the *irc5* translocase through cohesin. *EMBO J.*, **37**, e98732.
49. Feretzaki,M., Pospisilova,M., Valador Fernandes,R., Lunardi,T., Krejci,L. and Lingner,J. (2020) RAD51-dependent recruitment of TERRA lncRNA to telomeres through R-loops. *Nature*, **587**, 303–308.
50. Daza-Martin,M., Starowicz,K., Jamshad,M., Tye,S., Ronson,G.E., MacKay,H.L., Chauhan,A.S., Walker,A.K., Stone,H.R., Beesley,J.F.J. *et al.* (2019) Isomerization of BRCA1-BARD1 promotes replication fork protection. *Nature*, **571**, 521–527.
51. Koury,E., Harrell,K. and Smolikove,S. (2018) Differential RPA-1 and RAD-51 recruitment *in vivo* throughout the *C. elegans* germline, as revealed by laser microirradiation. *Nucleic Acids Res.*, **46**, 748–764.
52. Leon-Ortiz,A.M., Panier,S., Sarek,G., Vannier,J.B., Patel,H., Campbell,P.J. and Boulton,S.J. (2018) A distinct class of genome rearrangements driven by heterologous recombination. *Mol. Cell*, **69**, 292–305.
53. Stork,C.T., Bocek,M., Crossley,M.P., Sollier,J., Sanz,L.A., Chedin,F., Swigut,T. and Cimprich,K.A. (2016) Co-transcriptional R-loops are the main cause of estrogen-induced DNA damage. *Elife*, **5**, e17548.
54. Hamperl,S., Bocek,M.J., Saldivar,J.C., Swigut,T. and Cimprich,K.A. (2017) Transcription-replication conflict orientation modulates R-Loop levels and activates distinct DNA damage responses. *Cell*, **170**, 774–786.
55. Hicks,T., Koury,E., McCabe,C., Williams,C., Crahan,C. and Smolikove,S. (2022) R-loop-induced irreparable DNA damage evades checkpoint detection in the *C. elegans* germline. *Nucleic Acids Res.*, **50**, 8041–8059.
56. Derry,W.B., Putzke,A.P. and Rothman,J.H. (2001) Caenorhabditis elegans p53: role in apoptosis, meiosis, and stress resistance. *Science*, **294**, 591–595.
57. Schumacher,B., Hofmann,K., Boulton,S. and Gartner,A. (2001) The *c. elegans* homolog of the p53 tumor suppressor is required for DNA damage-induced apoptosis. *Curr. Biol.*, **11**, 1722–1727.
58. Gurumurthy,S., Xie,S.Z., Alagesan,B., Kim,J., Yusuf,R.Z., Saez,B., Tzatsos,A., Ozsolak,F., Milos,P., Ferrari,F. *et al.* (2010) The lkb1 metabolic sensor maintains haematopoietic stem cell survival. *Nature*, **468**, 659–663.
59. Gan,B., Hu,J., Jiang,S., Liu,Y., Sahin,E., Zhuang,L., Fletcher-Sananikone,E., Colla,S., Wang,Y.A., Chin,L. *et al.* (2010) Lkb1 regulates quiescence and metabolic homeostasis of haematopoietic stem cells. *Nature*, **468**, 701–704.
60. Horsley,V., Aliprantis,A.O., Polak,L., Glimcher,L.H. and Fuchs,E. (2008) NFATc1 balances quiescence and proliferation of skin stem cells. *Cell*, **132**, 299–310.
61. Hong,Y., Roy,R. and Ambros,V. (1998) Developmental regulation of a cyclin-dependent kinase inhibitor controls postembryonic cell cycle progression in caenorhabditis elegans. *Development*, **125**, 3585–3597.
62. Kadekar,P. and Roy,R. (2019) AMPK regulates germline stem cell quiescence and integrity through an endogenous small RNA pathway. *PLoS Biol.*, **17**, e3000309.
63. Shilatifard,A. (2012) The COMPASS family of histone H3K4 methylases: mechanisms of regulation in development and disease pathogenesis. *Annu. Rev. Biochem.*, **81**, 65–95.
64. Zardoni,L., Nardini,E., Brambati,A., Lucca,C., Choudhary,R., Loperfido,F., Sabbioneda,S. and Liberi,G. (2021) Elongating RNA polymerase II and RNA:DNA hybrids hinder fork progression and gene expression at sites of head-on replication-transcription collisions. *Nucleic Acids Res.*, **49**, 12769–12784.
65. Rao,R.C. and Dou,Y. (2015) Hijacked in cancer: the KMT2 (MLL) family of methyltransferases. *Nat. Rev. Cancer*, **15**, 334–346.
66. Butuci,M., Williams,A.B., Wong,M.M., Kramer,B. and Michael,W.M. (2015) Zygotic genome activation triggers chromosome damage and checkpoint signaling in *C. elegans* primordial germ cells. *Dev. Cell*, **34**, 85–95.
67. Wong,M.M., Belew,M.D., Kwieraga,A., Nhan,J.D. and Michael,W.M. (2018) Programmed DNA breaks activate the germline genome in *Caenorhabditis elegans*. *Dev. Cell*, **46**, 302–315.
68. Blythe,S.A. and Wieschaus,E.F. (2015) Zygotic genome activation triggers the DNA replication checkpoint at the midblastula transition. *Cell*, **160**, 1169–1181.
69. Roberts,S.A. and Gordenin,D.A. (2014) Hypermutation in human cancer genomes: footprints and mechanisms. *Nat. Rev. Cancer*, **14**, 786–800.
70. Ghalambor,C.K., Hoke,K.L., Ruell,E.W., Fischer,E.K., Reznick,D.N. and Hughes,K.A. (2015) Non-adaptive plasticity potentiates rapid adaptive evolution of gene expression in nature. *Nature*, **525**, 372–375.